

# Pulse shaping using dispersion-engineered difference frequency generation

M. Allgaier,<sup>1</sup> V. Ansari,<sup>1</sup> J. M. Donohue,<sup>1,2</sup> C. Eigner,<sup>1</sup> V. Quiring,<sup>1</sup> R. Ricken,<sup>1</sup> B. Brecht,<sup>1</sup> and C. Silberhorn<sup>1</sup>

<sup>1</sup>*Integrated Quantum Optics, Applied Physics, University of Paderborn, 33098 Paderborn, Germany*

<sup>2</sup>*Institute for Quantum Computing, University of Waterloo,  
200 University Ave. West, Waterloo, Ontario, Canada, N2L 3G1*

(Dated: December 20, 2018)

The temporal-mode (TM) basis is a prime candidate to perform high-dimensional quantum encoding. Quantum frequency conversion has been employed as a tool to perform tomographic analysis and manipulation of ultrafast states of quantum light necessary to implement a TM-based encoding protocol. While demultiplexing of such states of light has been demonstrated in the Quantum Pulse Gate (QPG), a multiplexing device is needed to complete an experimental framework for TM encoding. In this work we demonstrate the reverse process of the QPG. A dispersion-engineered difference frequency generation in non-linear optical waveguides is employed to imprint the pulse shape of the pump pulse onto the output. This transformation is unitary and can be more efficient than classical pulse shaping methods. We experimentally study the process by shaping the first five orders of Hermite-Gauss modes of various bandwidths. Finally, we establish and model the limits of practical, reliable shaping operation.

High-dimensional encoding can potentially increase the security of quantum communication protocols as well as the information capacity of a single photon [1, 2]. Orbital angular momentum (OAM) has been proposed as such a basis for high-dimensional encoding [3] but is inherently incompatible with existing telecommunication fiber networks. Temporal modes (TMs) of ultrafast pulses of light are a viable, fiber-compatible alternative to OAM, owing to their spatially single-mode nature [4]. The core of the TM framework is the Quantum Pulse Gate (QPG), a non-linear optical device based on dispersion-engineered quantum frequency conversion in non-linear waveguides [5]. The QPG has been shown to perform efficient sorting (i.e. demultiplexing) of the orthogonal but field-overlapping modes [6–12], as well as state manipulation and purification [9], photon subtraction [13, 14] and noise suppression [15]. Quantum light in TM basis can be directly generated using an adapted parametric down-conversion source [16]. For two-dimensional states, reshaping (i.e. modal rotation) has been explored [17]. However, an independent TM multiplexing device capable of arbitrary TM shaping and reshaping of higher order modes such as the Quantum Pulse Shaper (QPS) described in Ref. [18] has not been demonstrated, neither on the single photon level, nor classically. Such a device, together with a QPG, could perform rotations between TMs. The process can in principle be very efficient, contrary to established classical pulse shaping methods in the spectral [19] and time domain [20].

In this work we experimentally demonstrate a difference frequency generation (DFG) based pulse shaper and study its performance using coherent light. We verify successful shaping of the converted light into the first five orders of Hermite-Gauss modes using spectral intensity measurements. We assess the process' shaping accuracy by scanning the bandwidth of the desired spectrum and model experimental imperfections for comparison. We thus establish a range of working parameters for such a pulse reshaping device.

To design a DFG pulse shaping device such as the QPS, one has to first revisit the working principle behind the QPG. Key to the QPG device is its unique group-velocity relationship: By matching the group velocity of input and pump field in a sum-frequency generation (SFG) process, the conversion efficiency is directly proportional to the temporal overlap of the two fields, thus allowing to selectively convert field-orthogonal modes. This group-velocity matching has been achieved in two different ways: Using an almost degenerate type-0 non-linear process [10, 11], or by compensating for the waveguide's dispersion with material birefringence using a type-II process [18]. The latter has the prospect of better background suppression, resulting in signal-to-noise ratio sufficient for operating on quantum light [9]. This particular type-II implementation addresses inputs in the telecom band around 1550 nm and outputs them in the visible range around 557 nm. A QPS should ideally work in the opposite direction, thus enabling us to reconvert the output of a QPG to allow for TM rotations. Therefore, we propose to employ the reverse process of the QPG, i.e. difference-frequency generation (DFG). Here, using a type-II process is especially advantageous over type-0: The single photon output at 1550 nm for a type-0 process can be separated from its pump field only by a few nanometers, and therefore be polluted by Raman-scattered photons. The process is implemented in periodically poled Lithium Niobate waveguides. Employing the exact reverse process for SFG and DFG, i.e. same material, wavelengths and polarizations, allows the usage of the same waveguide structure and poling period. For group-velocity matched SFG, highly efficient bandwidth compression has already been demonstrated [21]. In an analog fashion, pulse shaping implemented in the DFG process can also be highly efficient, and even bandwidth expansion is possible, with potential applications in interfacing with narrowband photons.

For the DFG device presented here, a central pump wavelength of 1550 nm is chosen in order to convert nar-

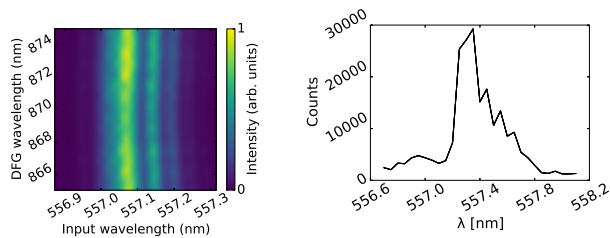


Figure 1. Left: DFG phasematching derived from the measured SFG phasematching. Right: Phasematching scan at a pump wavelength of 1550 nm

rowband light at 557 nm to 850 nm. This interchange of pump and output wavelength is possible due to the matched group-velocity, and the necessary lasers and classical pulse shapers were already available to the authors. From the SFG phasematching measured in a QPG configuration [21], we derive the corresponding DFG phasematching with the accordingly different input and output wavelength and show it in Figure 1. Directly scanning the phasematching in the DFG configuration was not possible due to poor repeatability of the 557 nm laser’s tuning, but a single scan through the phasematching verifies the derived phasematching. The experimental setup is shown in Figure 2. To generate the input light we rely on a diode-pumped solid state laser emitting at 514 nm to pump a standing-wave continuous wave dye laser. Rhodamine-560 is employed as a laser dye to generate the necessary wavelength of 557 nm. The laser’s emission bandwidth is typically of the order of 5 GHz. A pulsed laser at 550 nm was not available to the authors. The pump pulses are generated with a cascade of a Ti:Sapphire oscillator operating at 80 MHz repetition rate, and an optical parametric oscillator emitting pulses with a central wavelength of 1550 nm. The light is coupled to standard SMF-28 fibers and fed through a fiber-coupled spatial light modulator-based pulse shaper with a resolution of 10 GHz over the entire telecom C-band. The pulses are combined with the 557 nm input light on a dichroic mirror and coupled into a 27 mm long, home-made Titanium-indiffused Lithium Niobate waveguide with a poling period of  $4.4 \mu\text{m}$ . Input and pump pulses are orthogonally polarized since we are employing a type-II process. The converted light is separated from the input light and coupled to another single mode fiber. We employ a single-photon sensitive spectrometer with a resolution of 0.05 nm at 870 nm, provided by a 1200 lines/mm grating. For analysis, we calculate the expected DFG spectrum from the spectrum programmed on the pulse shaper. This is particularly simple due to the continuous wave input. We compare this spectrum to the measured one by means of an overlap integral. Unfortunately, with the available input and pump power, the generated pulses were too weak to characterize their spectral phase using classical pulse characterization techniques.

Light produced by parametric down-conversion sources

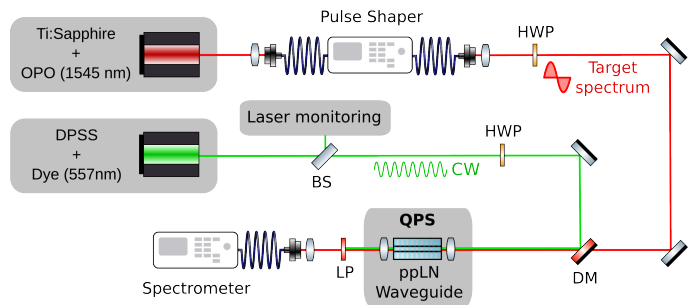


Figure 2. The experimental setup for device characterization. OPO: Optical parametric oscillator, DPSS: Diode pumped solid state laser, HWP: Half wave plate, Ti:ppLN: periodically poled Lithium Niobate, LP: Long pass filter

naturally decomposes into the Hermite-Gauss basis [22]. Since the device presented here is intended for use in the QPG framework, we choose exactly this basis. The spectral envelope of the pulses read:

$$HG_n(\lambda) = \frac{H_n(\lambda - \lambda_0)}{N_n} \cdot e^{-\frac{(\lambda - \lambda_0)^2}{2\sigma^2}} \quad (1)$$

where  $H_n$  denotes the Hermite polynomial of order  $n$ ,  $\lambda_0$  is the central wavelength, and  $\sigma$  denotes the base Gaussian’s bandwidth in the following, although the actual spectral spread will be higher for higher-order modes.  $N$  normalizes the Hermite-Gauss function. We scan the bandwidth of the underlying Gaussian from 0.25 nm to 10 nm in steps of 0.25 nm, and perform 8 measurements with 4 seconds integration time each for every set of parameters. The standard deviation over the mean value of the 8 measurements is used to generate error bars. Thus, for every Hermite-Gauss order 320 measurements are taken, this task is repeated for the first 5 orders of Hermite-Gauss modes over the course of half a day. For every bandwidth  $\sigma$ , we calculate the overlap between target and measured spectrum:

$$OL = \frac{(\int S(\lambda)T(\lambda)d\lambda)^2}{\int S^2(\lambda)d\lambda \cdot \int T^2(\lambda)d\lambda} \quad (2)$$

where  $S(\lambda)$  and  $T(\lambda)$  are the measured and programmed target spectra, respectively. The results are displayed in Figure 3.

The overlap between the measured programmed spectra are displayed in magenta. The achieved overlap is above 90 % over a large bandwidth range from about 1 to 6 nm for all five modes. The best overlap at over 95 % is achieved for bandwidths between roughly 3.5 and 5 nm. It is noteworthy that a higher order Hermite-Gauss mode of the same nominal bandwidth occupies a wider spectrum, since the Gaussian is scaled by the Hermite polynomial. This causes the steeper decline of the overlap for wider bandwidths and higher orders. To better understand these results, we modeled the experimental limitations of the current setup. The overlap between these

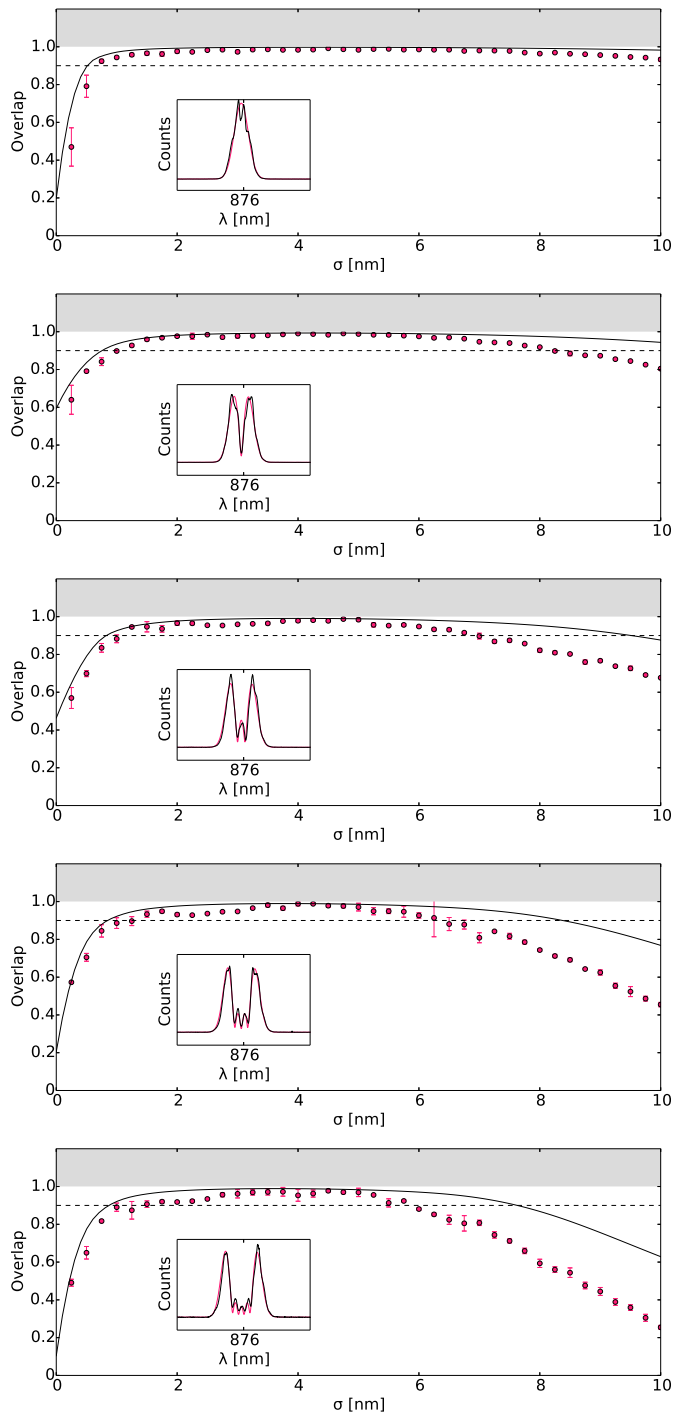


Figure 3. Overlap between the programmed and measured Hermite-Gauss spectra for the first five modes. The dashed lines indicate 95% overlap. Solid lines indicate the overlap between the programmed and modeled spectra, which include experimental limitations. The inserts show the programmed (magenta) and measured (black) spectra for each mode and a bandwidth of 5 nm.

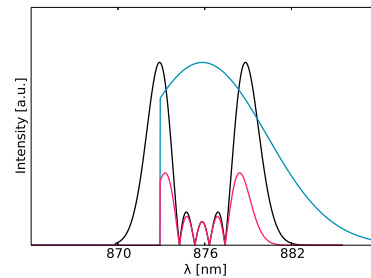


Figure 4. Sketched programmed spectrum (black), available pump spectrum with limited shaper range (blue) and resulting actual shaped spectrum (magenta) for a fourth order Hermite-Gauss mode.

modeled spectra and the programmed ones are again calculated and displayed as solid lines. The model contains two classes of contributions.

First, we account for insufficient available bandwidth at 1550 nm, which effectively narrows down the shaped spectrum. This includes three contributions: The available bandwidth from the pump laser, the available phase-matching bandwidth, and the range of the pulse shaper. While the first two contributions result in a combined Gaussian spectrum of 10 nm FWHM, with which the programmed spectrum is multiplied. Figure 4 shows this effect for the 4th order mode with a bandwidth of 10 nm. The black line is the programmed spectrum. However, it can only be carved within the operating bandwidth of the pulse shaper, and only from the Gaussian spectrum with limited bandwidth (shown in blue), which is why the actual shaped spectrum (magenta) looks different from the programmed one. The difference is mostly visible in the outer parts of the spectrum, which is why only large bandwidths and higher-order modes are affected.

Second, we model convolution effects. These are due to limited resolution of the employed pulse shaper (10 GHz) and spectrometer (20 GHz), as well as the non-negligible bandwidth of the dye laser (5 GHz). The programmed spectrum is convoluted with a Gaussian to account for these effects. Another such effect stems from multimode-ness of the dye laser, which experiences a certain degree of mode competition. The two modes of 5 GHz bandwidth are estimated to be about 0.1 nm apart. We account for this by adding up two spectra of the same separation. We estimate the ratio to be 1:1, since the mode competition takes place on the order of seconds, whereas the measurement for each bandwidth takes 32 seconds, thus averaging sufficiently over both mode contributions. These effects blur the spectrum, and lead to diminished overlap for small bandwidths.

It is apparent that the model does not fit well the large bandwidths, while the qualitative trend is still reproduced. We attribute this to instabilities in the spectra produced by the optical parametric oscillator. It is possible to observe fringing effects in the pump spectrum in front of the pulse shaper, manifesting as small features

in the spectra. In addition, the pump spectrum in front of the pulse shaper is not exactly Gaussian and exhibits some degree of asymmetry. These features change over time on a scale of 10 seconds and cause more pronounced deviations for more complex and wider spectra.

The individual contributions to the model are treated in more detail in the supplementary materials. From the achieved overlaps we conclude that the device works in principle, with some constraints imposed by the current experimental setup. However, it is important to dissect which of the imperfections are fundamental to the device, and which are only caused by auxiliary equipment such as the lasers. First, the spectrometer resolution is not a fundamental restriction for the device, since it only influences how well the shaped spectra can be characterized, not how well they are shaped. The effects imposed by the pulse shaper are device dependent. This leaves the 557 nm input bandwidth and phasematching bandwidth as ultimate limits to device performance. Therefore, we model the influences of these ultimate limitations on the proposed pulsed input device. The input bandwidth should always be chosen smaller or equal the phasematching bandwidth, or otherwise the spectrum will be cut and effectively filtered once more. We now assume a flat spectral intensity and phase of the pump laser spectrum, as well as a flat response of the pulse shaper. The pulse shaper's resolution of 10 GHz will be small compared to the phasematching bandwidth and neglected. Still, the non-zero input bandwidth results in a convolution effect just like the ones discussed above. Using those benchmark numbers, calculations identical to the model already presented were prepared to simulate the effect of the input and phasematching bandwidth on the quantum device performance. Since the highest order mode used is subject to the strongest limitations, we only show the results for the 4th order Hermite-Gauss mode in Figure 5. It can be seen that for a more narrow phasematching bandwidth than the one for the waveguide used in this work, shaping bandwidths under 1 nm is certainly possible. This would require longer waveguides. This is highly desirable in the light of optical fiber dispersion and spec-

tral information density. At the same time, high shaping fidelity for small bandwidth features would also allow us to shape higher order modes efficiently. The inset shows the target and model spectrum for a mode bandwidth of 1.8 nm and a phasematching bandwidth of 0.2 nm. The blurring effect on the central features can clearly be observed. This is the source of the diminished overlap.

In conclusion, we have shown the classical characterization of a DFG pulse shaper and show successful reshaping of the input light into Hermite-Gauss pulses of a broad substantial range of bandwidths. From the theoretical model of the experimental imperfections we draw the conclusion that a highly functional device for pulsed operation can be implemented using the current waveguide technology.

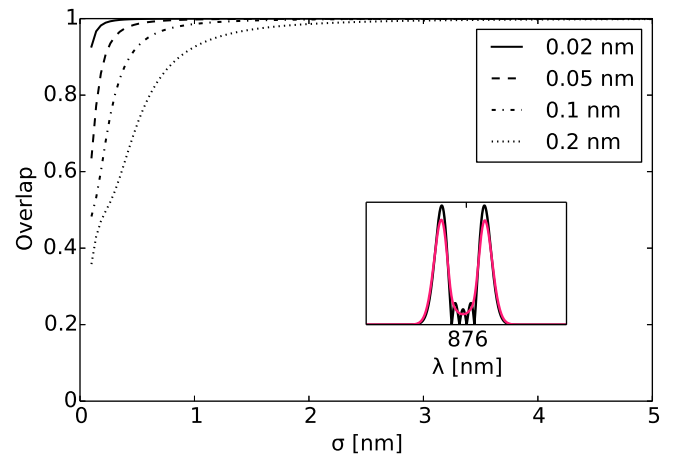


Figure 5. Overlap between the programmed and modeled spectra of the fourth Hermite-Gauss order for various phasematching bandwidths. The inset shows the target (black) and model (magenta) spectrum for a phasematching bandwidth of 0.2 nm and a mode bandwidth of 1.8 nm.

## ACKNOWLEDGEMENT

This work was funded by the DFG through the SFB TRR 142.

- 
- [1] Peter P. Rohde, Joseph F. Fitzsimons, and Alexei Gilchrist. Information capacity of a single photon. *Physical Review A*, 88(2):022310, August 2013.
- [2] Alex Hayat, Xingxing Xing, Amir Feizpour, and Aephraim M. Steinberg. Multidimensional quantum information based on single-photon temporal wavepackets. *Optics Express*, 20(28):29174–29184, December 2012.
- [3] J. Leach, B. Jack, J. Romero, A. K. Jha, A. M. Yao, S. Franke-Arnold, D. G. Ireland, R. W. Boyd, S. M. Barnett, and M. J. Padgett. Quantum Correlations in Optical Angle-Orbital Angular Momentum Variables. *Science*, 329(5992):662–665, August 2010.
- [4] B. Brecht, Dileep V. Reddy, C. Silberhorn, and M. G. Raymer. Photon Temporal Modes: A Complete Framework for Quantum Information Science. *Physical Review X*, 5(4):041017, October 2015.
- [5] Andreas Eckstein, Benjamin Brecht, and Christine Silberhorn. A quantum pulse gate based on spectrally engineered sum frequency generation. *Optics Express*, 19(15):13770–13778, July 2011.
- [6] D. V. Reddy, M. G. Raymer, C. J. McKinstrie, L. Mejling, and K. Rottwitt. Temporal mode selectivity by frequency conversion in second-order nonlinear optical waveguides. *Optics Express*, 21(11):13840–13863, June 2013.

- [7] Benjamin Brecht, Andreas Eckstein, Raimund Ricken, Viktor Quiring, Hubertus Suche, Linda Sansoni, and Christine Silberhorn. Demonstration of coherent time-frequency Schmidt mode selection using dispersion-engineered frequency conversion. *Physical Review A*, 90(3):030302, September 2014.
- [8] Vahid Ansari, Georg Harder, Markus Allgaier, Benjamin Brecht, and Christine Silberhorn. Temporal-mode measurement tomography of a quantum pulse gate. *Physical Review A*, 96(6):063817, December 2017.
- [9] Vahid Ansari, John M. Donohue, Markus Allgaier, Linda Sansoni, Benjamin Brecht, Jonathan Roslund, Nicolas Treps, Georg Harder, and Christine Silberhorn. Tomography and Purification of the Temporal-Mode Structure of Quantum Light. *Physical Review Letters*, 120(21):213601, May 2018.
- [10] Paritosh Manurkar, Nitin Jain, Michael Silver, Yu-Ping Huang, Carsten Langrock, Martin M. Fejer, Prem Kumar, and Gregory S. Kanter. Multidimensional mode-separable frequency conversion for high-speed quantum communication. *Optica*, 3(12):1300–1307, December 2016.
- [11] Dileep V. Reddy and Michael G. Raymer. Engineering temporal-mode-selective frequency conversion in nonlinear optical waveguides: from theory to experiment. *Optics Express*, 25(11):12952, May 2017.
- [12] Dileep V. Reddy and Michael G. Raymer. Temporal-mode-selective optical Ramsey interferometry via cascaded frequency conversion. *arXiv:1710.06736 [physics, physics:quant-ph]*, October 2017. arXiv: 1710.06736.
- [13] Valentin A. Averchenko, Valrian Thiel, and Nicolas Treps. Nonlinear photon subtraction from a multimode quantum field. *Physical Review A*, 89(6), June 2014.
- [14] Young-Sik Ra, Clément Jacquard, Adrien Dufour, Claude Fabre, and Nicolas Treps. Tomography of a Mode-Tunable Coherent Single-Photon Subtractor. *Physical Review X*, 7(3), July 2017.
- [15] Amin Shahverdi, Yong Meng Sua, Lubna Tumeh, and Yu-Ping Huang. Quantum Parametric Mode Sorting: Beating the Time-Frequency Filtering. *Scientific Reports*, 7(1), December 2017.
- [16] V. Ansari, E. Roccia, M. Santandrea, M. Doostdar, C. Eigner, L. Padberg, I. Gianani, M. Sbroscia, J. M. Donohue, L. Mancino, M. Barbieri, and C. Silberhorn. Heralded generation of high-purity ultrashort single photons in programmable temporal shapes. *Optics Express*, 26(3):2764–2774, February 2018.
- [17] Paritosh Manurkar, Nitin Jain, Prem Kumar, and Gregory S. Kanter. Programmable optical waveform reshaping on a picosecond timescale. *Optics Letters*, 42(5):951–954, March 2017.
- [18] Benjamin Brecht, Andreas Eckstein, Andreas Christ, Hubertus Suche, and Christine Silberhorn. From quantum pulse gate to quantum pulse shaper-engineered frequency conversion in nonlinear optical waveguides. *New Journal of Physics*, 13(6):065029, June 2011.
- [19] Andrew M. Weiner. Ultrafast optical pulse shaping: A tutorial review. *Optics Communications*, 284(15):3669–3692, July 2011.
- [20] C. E. Rogers and P. L. Gould. Nanosecond pulse shaping at 780 nm with fiber-based electro-optical modulators and a double-pass tapered amplifier. *Optics Express*, 24(3):2596, February 2016.
- [21] Markus Allgaier, Vahid Ansari, Linda Sansoni, Christof Eigner, Viktor Quiring, Raimund Ricken, Georg Harder, Benjamin Brecht, and Christine Silberhorn. Highly efficient frequency conversion with bandwidth compression of quantum light. *Nature Communications*, 8:14288, January 2017.
- [22] S P Walborn and A H Pimentel. Generalized Hermite-Gauss decomposition of the two-photon state produced by spontaneous parametric down conversion. *Journal of Physics B: Atomic, Molecular and Optical Physics*, 45(16):165502, August 2012.